2020-06-04

A System for Foot Joint Kinetics – Integrating Plantar Pressure/ Shear with Multisegment Foot Modeling

Spencer Ray Petersen
Brigham Young University

A System for Foot Joint Kinetics – Integrating Plantar Pressure/Shear with Multisegment Foot Modeling

Spencer Ray Petersen

A thesis submitted to the faculty of
Brigham Young University
in partial fulfillment of the requirements for the degree of

Master of Science

Dustin A. Bruening, Chair
Matthew K. Seeley
Sarah T. Ridge

Department of Exercise Sciences

Brigham Young University

ABSTRACT

A System for Foot Joint Kinetics – Integrating Plantar Pressure/Shear with Multisegment Foot Modeling

Spencer Ray Petersen
Department of Exercise Sciences, BYU
Master of Science

Introduction: Instrumented gait analysis and inverse dynamics are commonly used in research and clinical practice to calculate lower extremity joint kinetics, such as power and work. However, multisegment foot (MSF) model kinetics have been limited by ground reaction force (GRF) measurements. New technology enables simultaneous capture of plantar pressure and shear stress distributions but has not yet been used with motion capture. Integrating MSF models and pressure/shear measurements will enhance the analysis of foot joint kinetics. The purpose of this study was to develop methodology to integrate these systems, then analyze the effects of speed on foot joint kinetics.

Methods: Custom software was developed to synchronize motion capture and pressure/shear data using measured offsets between reference frame origins and time between events. Marker trajectories were used to mask pressure/shear data and construct segment specific GRFs. Inverse dynamics was done in commercial software. Demonstrative data was from 5 healthy adults walking unshod at 3 fixed speeds (1.0, 1.3, and 1.6 m/s, respectively) wearing retroreflective markers according to an MSF model. Plantar shear forces and ankle, midtarsal, and first metatarsophalangeal (MTP) joint kinetics were reported. Speed effects on joint net work were evaluated with a repeated measures ANOVA.

Results: Plantar shear forces during stance showed some spreading effects (directionally opposing shear forces) that relatively were unaffected by walking speed. Midtarsal joint power seemed to slightly lag behind the ankle, particularly in late stance. Net work at the ankle ($p = 0.024$), midtarsal ($p = 0.023$), and MTP ($p = 0.009$) joints increased with speed.

Conclusions: Functionally, the ankle and midtarsal joints became more motorlike with increasing speed by generating more energy than they absorbed, while the MTP joint became more damperlike by absorbing more energy than it generated. System integration appears to be an overall success. Limitations and suggestions for future work are presented.

Keywords: plantar mask, motion capture, force partition, instrumented gait, energetics

TABLE OF CONTENTS

LIST OF FIGURES

Introduction

Instrumented gait analysis is a commonly used tool in both basic research and clinical practice. Joint kinetics, such as net moments and powers, are derived through inverse dynamics by integrating motion capture technology with force measurements (Baker, 2007). These joint level parameters can help infer muscle activity and/or passive tissue resistance to movement (Andriacchi & Strickland, 1986). For instance, joint moments and powers produced by muscle activity (Zajac et al., 2002a) can reveal whether the active muscle group contributes to pathology or risk of injury (Scott & Winter, 1993). The time integral of joint power or joint work provides valuable insight into the energetic contributions of muscle groups crossing major joints (Zajac et al., 2002b; Olney, 1991). Joint kinetics has traditionally been confined to the analysis of major lower extremity joints (hip, knee, and ankle), yet it may have utility when applied to smaller joints, particularly those in the foot.

The foot has been a challenging area to research thoroughly due to its small size and complex nature. The traditional single segment foot model with a point load ground reaction force (GRF) does not model joints distal to the ankle and is therefore insufficient to measure internal foot mechanics (De Ridder et al., 2015; Leardini & Caravaggi, 2017). To tackle this issue, multisegment foot (MSF) models have been created ranging between two and nine segments (Deschamps et al., 2011). Most of these models have focused only on kinematics. While kinematic modeling is useful, kinetic models of the foot are necessary for inverse dynamics. Only a handful of kinetic MSF models have been presented in the literature (Bruening et al., 2012a; MacWillimas et al., 2003; Deschamps et al., 2011; Dixon et al., 2012); all of these have suffered from technological limitations that prevent their adoption in clinical practice (Buczek et al., 2006; Bruening & Takahashi, 2018).

The measurement of ground reaction forces under individual segments of the foot is the biggest hurdle in creating kinetic MSF models. For inverse dynamics, GRF must be measured for each segment of the model in contact with the ground. Force plates provide a single net force vector for the entire surface of the plate, regardless of how many segments are in contact with it. The few studies that have attempted to measure segment GRFs approached the problem using three methods. First, partitioning from a single force plate by applying the entire measured GRF sequentially to segments once the center of pressure is anterior to the proximal end of the segment (Stefanyshyn & Nigg, 1997). Second, partitioning from a single force plate by applying part of the measured GRF to individual segments proportional to pressure distributions (Giacomozzi & Macellari, 1997; MacWillimas et al., 2003). Finally, using multiple adjacent force plates to measure segment GRFs (Bruening et al, 2012b). These methods rely on assumptions about the way in which the GRF is distributed. The sequential application method assumes that total force acts on only one segment at a time. The pressure partitioning method assumes that horizontal shear stress distributions are proportional to vertical pressure distributions and that there are no opposing shear forces between segments (Bruening & Takahashi, 2018). The adjacent force plates method is limited to measuring at most two segments at a time and relies on consistent foot placement during gait which is not always clinically feasible. These methods and their limitations have previously been evaluated in greater detail by Bruening and Takahashi (2018).

A direct measurement of segment GRFs, when integrated with motion capture, will advance multisegment kinetic foot modeling, allow for the application of inverse dynamics to multiple foot joints, increase our understanding of foot intrinsic muscle activity and energetic contributions, and help clinicians better treat pathologies affecting the foot. Recent advances in

shear sensing technology have created opportunities to directly measure plantar force distributions (Goss et al., 2019). While this technology has been used previously to analyze shear stresses in diabetic gait (Stucke et al., 2012), it has not yet been integrated with motion capture and foot modeling. The primary purpose of this study was to develop a new system for MSF inverse dynamics calculations by combining 3D motion capture with a plantar pressure and shear sensor.

The utility of the proposed system was demonstrated by calculating and presenting net joint moments, powers and work done for the ankle, midtarsal, and first metatarsophalangeal (MTP) joints across 3 distinct walking speeds. Gait speed has been shown to have a large effect on joint kinematics and kinetics (Schwartz et al., 2008), and changes in gait speed are often used to systematically probe and study the energetics of human gait (Farris & Sawicki, 2012; Zelik, Takahashi, & Sawicki, 2015; Ebrahimi et al., 2017; Kuhman & Hurt., 2019; Neptune et al., 2008). Thus, a secondary purpose of this work was to preliminarily study the effects of walking speed on multisegment foot joint kinetics. This work will result in initial insights into the manner in which the foot joints absorb, generate, and transfer energy needed for ambulation as well as provide the foundation for a normative database that can be used as a comparison in clinical gait analysis. We hope that the overall framework presented will be a catalyst in advancing the study of multisegment foot kinetics.

System Integration

Measurement Equipment

Pressure/shear data were collected with a plantar distribution sensor (FootSTEPS, ISSI, Dayton, OH, USA). This sensor consists of a stress-sensitive film, a camera, and a force plate. As subjects walk across the device, the film of the sensor is displaced and optically measured by the camera. Film displacements are converted to vertical pressure, mediolateral and anteroposterior shear stress distributions using a finite element analysis developed by ISSI. A force plate (AMTI, Watertown MA, USA) mounted underneath the device is used for calibration. The camera measures a 0.42 by 0.28 meter rectangle and is limited to a 50 Hz sampling rate, while the force plate is sampled at a much higher 1000 Hz. Details regarding the device hardware and measurement validity are presented by Goss et al. (2019). The device is 64.8 cm tall and not easily mounted in-ground, thus a 5.5 m long walkway was created using three 1.8 m x 0.9 m adjustable height staging panels (StageRight Z-HD, Clare, MI, USA). A hole was cut in the center panel for the sensor and a small (< 1 cm) gap was maintained around the device perimeter (Figure 1).

Motion data were collected with a 10-camera motion capture system (Qualisys, Gottberg, Sweden) at 100Hz. Nineteen retroreflective markers were adhered to subject's feet according to a previously presented kinetic MSF model (Bruening et al., 2012a) with a few modifications. This model defines shank, hindfoot, forefoot, and hallux segments which are separated by ankle, midtarsal, and MTP joints, respectively. Marker locations and segment definitions are detailed in the Appendix.

System Alignment

Temporal and spatial alignment were required to combine motion capture with pressure/shear. Alignment was accomplished by measuring an offset between motion capture and pressure/shear. Temporal alignment occurred by measuring a time offset between a trigger signal (square wave falling edge TTL) from motion capture software to the pressure/shear collection software followed by subsequent square wave TTL trigger signal from the force plate hardware to the same collection software. The time elapsed between triggers was recorded and used in data processing. Spatial alignment was accomplished in two steps. The first oriented the motion capture and pressure/shear reference frames during motion capture calibration by placing the "L-frame" on one corner of the FootSTEPS device (Figure 2). This oriented two axes of each reference frame parallel to one another. The second measured the offset between reference frame origins by pressing a digitizing pointer with known motion capture coordinates against the surface of the device. As the film is compressed by the digitizing pointer the center of pressure is measured. The mean difference between pointer tip coordinates and center of pressure coordinates was recorded and used to align reference frame origins.

Data Processing

Custom LabView software (National Instruments, Austin, TX, USA) was used to implement algorithms to construct GRF for inverse dynamics calculations of the hindfoot, forefoot, and hallux segments. This construction occurs in 4 steps: Trial Synchronization; Dynamic Pressure Scaling; Segment Masking; and GRF Construction (Figure 3). Following GRF construction MSF modeling and inverse dynamics calculations are done in Visual 3D.

Trial Synchronization

Motion capture and pressure/shear data were synchronized in the custom software using the identified offsets. First, in order to match the number of samples in each set of data, pressure/shear data were up sampled from 50 Hz to 100 Hz and force plate data were down sampled from 1000 Hz to 100 Hz while motion capture data was collected at 100 Hz. Spatial synchronization was accomplished by projecting marker trajectories downwards onto the plane of the pressure/shear sensor film and transforming from the motion capture coordinate system to the pressure/shear coordinate system using the previously measured offset. Temporal synchronization was accomplished using the time offset measured by FootSTEPS software during system alignment. This offset, determined with a set of triggers, indicates the time elapsed between the onset of motion capture collection and heel strike. However, sometimes FootSTEPS triggered early so an optional workaround was developed. A heel strike event in pressure/shear data was detected by applying a 5 Newton threshold to the vertical force measured by the force plate. The same event in motion capture data was detected by thresholding the sagittal plane velocity of the heel marker (Bruening & Ridge, 2014). The user confirmed temporal synchronization in the software before data processing continued by comparing the time delay offset to the event detection algorithms.

Dynamic Pressure Scaling

While the stress-sensitive film captures raw shear stresses accurately, raw vertical pressure contains some inherent error. However, these errors were overcome using the force plate, as suggested by Goss et al. (2019). Each pixel of the camera image records a value indicating pressure, the force measured by the image is the sum of pressure multiplied by the area (see GRF Construction [1]). A conversion ratio, or scaling factor, was calculated by

comparing camera-measured force to the force plate. Each pixel was then multiplied by this scaling factor. This preserves the relative pressures of each image while adjusting the magnitude of pressure, so the sum of pressure multiplied by area exactly matches the force plate. This was done for each image collected thereby creating a dynamic constant, or conversion ratio (Goss et al., 2019).

In order to dynamically scale the vertical pressure, the region of the whole foot was extracted from a composite footprint image (Figure 4A). This composite image was created by retaining the maximum pressure values recorded by each pixel across time. Extracting the area of the whole foot from the footprint data was an automated process using marker trajectories. A reference frame for the foot was created and a rectangular region that encompassed the entire foot was fit to it. An anterior/posterior (A/P) axis was defined using the heel and dorsal metatarsal head markers followed by a medial/lateral (M/L) axis defined from the cross product of the A/P axis and the vertical axis of the lab. The rectangle length was scaled to 140% of A/P axis length and 200% of the width of the foot measured as the distance between dorsal and lateral metatarsal head markers. The length and width of this region were arbitrarily chosen to ensure the whole foot was encompassed based on pilot data. All vertical data outside of this rectangular region was assigned the value of zero in order to minimize any spurious pressure data. Finally, all pressure values in this region were then collectively scaled and matched to the force plate using a dynamic constant as suggested (Goss et al., 2019) (Figure 4B).

Segment Masking

Partitioning, or masking, footprint images into regions of interest is a common plantar pressure analysis technique. In this study, segment regions of interest that match model segments were automatically masked using an anatomical masking method (Giacomozzi & Stebbins,

2017). This method projected motion capture marker positions at mid-stance downward onto the plane of a composite footprint image. These points were used as vertices of segment regions of interest. Straight lines between points excluded valid portions of the footprint that pertain to the segment (Figure 5); therefore, manual masking, or visual inspection, was used to adjust the regions of interest for every trial to include areas that were excluded with anatomical masking.

GRF Construction

Force, center of pressure, and free moment for each foot segment were calculated using pressure and shear data contained within the segment region of interest. Vertical and shear forces for each segment (F_{seg}) were determined as the sum of the products of pixel pressure or shear (P_i) and the square area of the pixel (A_i) [1]. The center of pressure for each segment (CoP_{seg}) was calculated as the weighted average of pixel locations (X_i and Y_i} [2]. The free moment for each segment (M_{seg}) was calculated as the sum of the shear force moments about the center of pressure [3].

[1] $$F_{seg} = \Sigma(P_i * A_i)$$

[2] $$CoP_{Xseg} = \frac{\Sigma(X_i * F_{Zi})}{\Sigma F_{Zi}} \qquad CoP_{Yseg} = \frac{\Sigma(Y_i * F_{Zi})}{\Sigma F_{Zi}}$$

[3] $$M_{seg} = \Sigma R_{CoPi} \, X \, F_{XYi}$$

Modeling and Inverse Dynamics

Multisegment foot modeling and inverse dynamics calculations were performed in Visual 3D software (C-Motion, Germantown, MD, USA) by importing standard motion capture files and GRF data calculated as detailed above (see Data Processing). The latter was exported as an ASCII file and imported using Visual 3D pipeline commands. A static pose was used to model shank, hindfoot, forefoot, and hallux segments, as detailed in the Appendix. Dynamic motion data and force plate data prior to dynamic scaling were passed through a fourth order

Butterworth filter with cutoff frequencies of 6 Hz and 30 Hz. GRFs were then assigned to their respective segments and inverse dynamics calculated.

System Demonstration

Methods

Data from 5 healthy participants (3 Males, 2 Females, 24.2 ± 1.8 yrs, 1.77 ± 0.1 m, 77.6 ± 14.9 kg) were used to demonstrate system utility. Each participant signed an informed consent approved by the institutional review board at Brigham Young University. After motion capture markers were applied to their feet, participants were instructed to walk the length of the walkway at 3 fixed walking speeds (1.0 m/s, 1.3 m/s, 1.6 m/s). The speed of each subject was monitored with timing lights (Brower, Salt Lake City, UT, USA) and each trial had to be within ± 0.02 m/s of the target speed in order to be considered successful. The starting position was adjusted by researchers to prevent targeted foot placement. At least 3 trials with successful speeds and foot placement were collected for each speed.

All trials were processed using the previously described framework (see Data Processing). While primary analysis focused on joint kinetics, shear forces by themselves were also presented in a novel way to visualize opposing shear forces. For this analysis, all directional shear stresses were summed and multiplied by the area to create directional shear GRFs. Specifically, anterior directed shear stresses were separated from posterior directed shear stresses; likewise, medial and lateral shear stresses were separated from each other. The mean shear force in each respective direction was plotted across stance on the same graph as the counterpart force in order to provide a visual indicator of the amount of plantar tissue 'dragging' (unidirectional) and 'spreading' (bidirectional) as termed by Stucke et al. (2012). The effects of walking speed were visualized by plotting mean curves for all three speeds on the same graph.

Joint powers were also calculated and similarly presented across stance phase, with mean curves for each speed plotted on the same graph. Positive and negative work were calculated by integrating positive and negative portions of the power curves by time. Mean positive and negative work performed at each joint were calculated and plotted across speeds. The net work (sum of positive and negative work) was chosen to statistically evaluate the effects of walking speed on joint energetics. A repeated measures ANOVA ($\alpha = 0.05$) was run for the net work at each joint (across speeds) using JASP statistical software (JASP, Amsterdam, The Netherlands).

Results

A/P shear forces (Figure 6A) were primarily dragging during early (posterior) and late (anterior) stance. Some spreading effects were seen in midstance, with the greatest spreading forces during the transition from braking to propulsion. Speed had a notable effect on the peak braking and propulsive dragging forces but had little effect on overall spreading forces. Medial/Lateral (M/L) shear forces (Figure 6B) showed relatively consistent spreading effects throughout stance, with lateral shear forces equal to nearly half of the medial forces. However, speed appeared to have very little influence on M/L plantar spreading.

Ankle and midtarsal joint power waveforms (Figure 7) displayed similar characteristics, with power absorption through early and midstance, transitioning to power generation in late stance. The timing of peak power generation and the transition between negative and positive power were slightly earlier at the ankle compared with the midtarsal joint. At the MTP joint (Figure 7C), power absorption occurred concurrently with power generation at the ankle and midtarsal joints, followed by a small amount of power generation.

Speed appeared to have considerable effects on power profiles and work values in late stance for all joints and early stance at the ankle. At the ankle, as speed increased, the transition

from negative to positive power occurred earlier and peak power generation increased. However, the timing of this peak remained relatively unaffected. At the midtarsal joint a similar but less pronounced trend was observed. At the MTP joint peak powers (positive and negative) appeared to increase with speed but timing was relatively unaffected. Work values at the ankle and midtarsal joints visibly trended towards a decrease in negative work and an increase in positive work (Figure 8). Negative and positive work at the MTP joint both appeared to increase. Ankle joint net work was slightly negative at the slowest speed but became positive with increasing speed. Midtarsal joint net work was consistently positive, while MTP joint work was consistently negative. Statistically, net work at all three joint showed significant main effects, with ankle ($p = 0.024$) and midtarsal ($p = 0.023$) increasing positively and MTP increasing negatively ($p = 0.009$).

Discussion

The purpose of this demonstration was to evaluate speed effects on joint kinetics using an integrated motion capture and plantar pressure/shear sensor. While this was a pilot analysis, several insights were apparent.

Plantar shear stress distributions are currently untapped sources of potentially informative energetic data. Like plantar pressure, these distributions contain large quantities of data that need to be simplified for interpretation. Plantar pressure simplification often includes composite images and region-of-interest metrics such as peak pressure and pressure-time integrals. In contrast with pressure distributions, shear distributions are bidirectional. We leveraged this feature to create time-series graphs representing total force in each direction (Figure 6). Forces oriented in the opposite directions, termed ‘spreading’ (Stucke et al., 2012), indicate a dissipation of mechanical energy due to friction. A/P spreading occurs in midstance when the hindfoot and

forefoot segments are both in contact with the ground. This simultaneous contact of both ends of the medial longitudinal arch of the foot combined with compression from vertical loading likely produced this spreading effect by pushing the heel backwards and toes forward. M/L spreading was present throughout stance indicating that the transverse arch was constantly in compression. Late in stance, the M/L spread of the transverse arch reaches a maximum and loads the 2nd and 3rd metatarsal heads (Suzuki et al., 2004). This M/L spreading may play a role in balance and proprioception by stimulating mechanoreceptors (Morasso & Schieppati, 1999). Previous studies have suggested that these spreading forces may be an indicator of plantar ulceration (Stucke et al., 2012). Other foot deformities such as midfoot break or hallux valgus may also show substantial changes in A/P and M/L plantar spreading.

Speed appeared to have little effect on plantar spreading. Despite vertical force at midstance decreasing with speed (Schwartz et al., 2008), A/P spreading remained unchanged. M/L spreading occurred throughout stance with only subtle speed changes that may reflect, to a small degree, similar changes in the vertical GRF with speed. This seeming lack of response to speed may benefit clinicians by minimizing concerns regarding walking speed and pathological gait. Plantar spreading may be beneficial in other clinical applications such as surgical analysis of foot deformities. One simple way to quantify this spreading effect would be to report the magnitude of the nondominant (lesser magnitude) shear force using a simple algorithm to determine which force is nondominant and report its value.

Mechanical energy was absorbed and generated at the ankle, midtarsal and MTP joints. Ankle and midtarsal joints reflect the actions of each other very closely and absorb energy from the beginning of stance until late stance. Little is known about how positive midtarsal joint power is generated. The most likely sources are foot muscles (Kelly et al., 2019) and connective

tissues that cross the joint. Extrinsic muscles include the tibialis posterior and long toe flexors; intrinsic muscles include the short toe flexors, abductor hallucis, and abductor digit minimi. Connective tissues such as the plantar aponeurosis and intrinsic ligaments can passively contribute to propulsive energy by either storing and returning energy or by transferring energy from the MTP joint via the windlass mechanism (Bruening et al., 2018). The MTP joint appears to be mostly absorptive which is traditionally considered lost energy (Stefanyshyn & Nigg, 1997). The consistent timing of peak energy absorption, transition, and generation may be evidence that at least some of the energy is transferred via the windlass mechanism.

The effects of speed on joint level kinetics were most noticeable during late stance. The midtarsal joint seems to mimic the ankle joint in terms of power transition timing and peak power trends as speed increased, with some key differences. These similarities and differences are likely due to their proximity and shared energy contributing tissues. The differences between ankle and midtarsal power, such as later peak power generation, are likely magnified by intrinsic muscles and ligaments that cross the midtarsal joint but not the ankle, such as the flexor digitorum brevis and the long plantar ligament. These distal tissues may be continuing to influence the midtarsal joint after more proximal tissues have reduced their contributions. MTP power absorption was concurrent with ankle and midtarsal power generation and increased with speed, likely the result of an increase in joint angular velocity. As peak power absorption occurred, the transverse arch spreads and the 2nd and 3rd metatarsal heads were loaded for the remainder of push-off. This likely represents a balancing effect that may be magnified with increasing speed. MTP power generation also increased slightly with speed. This may be due to increased toe flexor muscle activation, perhaps with some contribution from tendon energy storage and return.

One viewpoint on joint function contrasts the negative work with the positive work immediately following (Kuhman & Hurt, 2019). Joints with small amounts of negative work followed by large amounts of positive work are considered to act like motors, while joints with somewhat equal positive and negative work are considered to act more like springs. Using this perspective, the ankle appears to become more motorlike with increasing speed as negative work decreases and positive work increases. The midtarsal joint follows a similar trend. This suggests that a reliance on active muscle contractions over passive energy sources may be more important at higher speeds. In contrast, the MTP joint produces a large amount of negative work followed by a small amount of positive work, suggesting a damping function that increases with speed. One limitation to this viewpoint is that interconnections between joints are not accounted for. For instance, if the windlass mechanism (the tightening of plantar tissues during toe extension) is responsible for a substantial portion of energy transfer between the MTP and midtarsal joints, then increases in negative MTP work and positive midtarsal work may be related, explaining their similar changes with walking speed.

Conclusions

The purposes of this study were to develop a new system for measuring multisegment foot joint kinetics by integrating direct pressure/shear measurements with motion capture and demonstrate the effects of speed on joint level parameters. While primary efforts of this paper were centered around integration methodology joint parameters were also reported and results did yield some preliminary insights into foot energetics showing overall success of the system.

Early integration of these devices was not without limitations. Temporal synchronization with hardware and software triggers were inconsistent. For this reason, creative workarounds had to be implemented in order to time synchronize motion capture and pressure/shear data. The

time-offset measurement was not relied on in this pilot study. Instead these two sets of data were synchronized by thresholding force plate data and motion event detection algorithms (Bruening & Ridge, 2014). After data collection for this study, communication with ISSI was continued and the pressure/shear data collection software has been patched to correct trigger signal issues. Future studies with this technology should no longer require this workaround. However, the pressure/shear device can still trigger early so the workaround will be maintained for future users.

The finite element analysis models used by ISSI to convert images of the stress-sensitive film to pressure/shear distributions require an exorbitant amount of time. Preprocess time can be reduced by scheduling batches of trials; however, the time reduction is minimal. This presents an additional hurdle to overcome before this system can become useful in more time-sensitive settings. Future collaborative efforts with ISSI will include methods to reduce preprocessing time.

Manual masking was used to adjust and finalize segment regions of interest in this pilot data set. Our preliminary efforts to implement anatomical masking did not identify the exact borders of the segments. For this small data set manual adjustments were not overburdening; however, for larger data sets automatic masking will be much more beneficial. Enhanced automated segment masking might be accomplished by implementing principles of machine vision or customizing a searching algorithm.

There were a few limitations associated specifically with demonstration of speed effects on joint kinetics. The sample size was small as this was a pilot study designed to show feasibility. Marker placement was performed by a few research assistants, which may have introduced some intersubject variance. The length of the walkway may have been slightly too

short for the fastest speed, introducing some challenges in capturing consistent walking speeds. Finally, statistical treatment was limited to one set of analysis. Joint net work was chosen because it is considered a summary representation of energetics.

Overall, the integrated system was determined to be successful. For the first time, motion capture and plantar pressure/shear measurements have been brought together for direct multisegment foot model kinetics. Plantar shear forces were visualized and contrasted in a new way. Lastly, preliminary speed effects on MSF energetics were investigated.

References

Andriacchi, T. P. & Strickland, A. B. (1986). Gait analysis as a tool to assess joint kinetics. *Biomechanics of Normal and Pathological Human Articulating Joints*, 83-102. doi:https://doi.org/10.1007/978-94-009-5117-4_5

Baker, R. (2007). The history of gait analysis before the advent of modern computers. *Gait & Posture, 26*, 331-342. doi:http://dx.doi.org/10.1016/j.gaitpost.2006.10.014

Bruening, D. A. & Ridge, S. T. (2014). Automated event detection algorithms in pathological gait. *Gait & Posture, 39*(1), 472-477. doi:https://doi.org/10.1016/j.gaitpost.2013.08.023

Bruening, D. A. & Takahashi, K. Z. (2018). Partitioning Groud Reaction Forces for Multi-Segment Foot Kinetics. *Gait & Posture, 62*, 111-116. doi:https://doi.org/10.1016/j.gaitpost.2018.03.001

Bruening, D. A., Cooney, K. M., & Buczek, F. L. (2012a). Analysis of a kinetic multi-segment foot model. Part I: Model repeatability and kinematic validity. *Gait & Posture,* (35), 529-534. doi:https://doi.org/10.1016/j.gaitpost.2011.10.363

Bruening, D. A., Cooney, K. M., & Buczek, F. L. (2012b). Analysis of a kinetic multi-segment foot model part II: Kinetics and clinical implications. *Gait & Posture, 35*(4), 535-540. doi:https://doi.org/10.1016/j.gaitpost.2011.11.012

Bruening, D. A., Pohl, M. B., Takahashi, K. Z., & Barrios, J. A. (2018). Midtarsal locking, the windlass mechanism, and running strike pattern. *Journal of Biomechanics, 73*, 181-195. doi:https://doi.org/10.1016/j.jbiomech.2018.04.010

Buczek, F. L., Walker, M. R., Rainbow, M. J., Cooney, K. M., & Sanders, J. O. (2006). Impact of mediolateral segmentation on a multi-segment foot model. *Gait & Posture, 23*(4), 519-522. doi:https://doi.org/10.1016/j.gaitpost.2005.06.004

De Ridder, R., Willems, T., Vanrenterghem, J., Robinson, M. P., & Roosen, P. (2015). Multisegment foot landing kinematics in subjects with chronic ankle instability. *Clinical Biomechaincs, 30*(6), 585-592. doi:https://doi.org/10.1016/j.clinbiomech.2015.04.001

Deschamps, K., Staes, F., Roosen, P., Nobels, F., Desloovere, K., Bruyninckx, H., & Matricali, G. A. (2011). Body of evidence supporting the clinical use of 3D multisegment foot models: A systematic review. *Gait & Posture*. doi:http://dx.doi.org/10.1016/j.gaitpost.2010.12.018

Dixon, P. C., Bohm, H., & Doderlein, L. (2012). Ankle and midfoot kinetics during normal gait: A multi-segment approach. *Journal of Biomechanics*, 1011-1016. doi:dx.doi.org/10.1016/j.jbiomech.2012.01.001

Ebrahimi, A., Goldberg, S. R., & Stanhope, S. J. (2017). Changes in relative work of the lower extremity joints and distal foot with walking speed. *Journal of Biomechanics, 58*, 212-216. doi:https://doi.org/10.1016/j.jbiomech.2017.04.012

Farris, D. & Sawicki, G. (2012). The mechanics and energetics of human walking and running: a joint level perspective. *Journal of The Royal Society Interface, 9*(66), 110-118. doi:https://doi.org/10.1098/rsif.2011.0182

Giacomozzi, C. & Macellari, V. (1997). Piezo-dynamometric platform for a more complete analysis of foot-to-floor interaction. *Transactions on Rehabilitation Engineering, 5*(4), 322-330. doi:https://doi.org/10.1109/86.650285

Giacomozzi, C. & Stebbins, J. A. (2017). Anatomical masking of pressure footprints based on the Oxford Foot Model: validation and clinical relevance. *Gait & Posture*, 131-138. doi:https://doi.org/10.1016/j.gaitpost.2016.12.022

Goss, L. P., Crafton, J. W., Davis, B. L., McMillan, G. R., Berki, V., Howe, A. E., & Papp, M. (2019). Plantar Pressure and Shear Measurement using Surface Stress Sensitive Film. *Measurement Science and Technology*. doi:doi.org/10.1088/1361-6501/ab4453

Kelly, L. A., Farris, D. J., Cresswell, A. G., & Lichtwark, G. A. (2019). Intrinsic foot muscles contribute to elastic energy storage and return in the human foot. *Journal of Applied Physiology, 126*(1), 231-238. doi:https://doi.org/10.1152/japplphysiol.00736.2018

Kuhman, D. J. & Hurt., C. P. (2019). Lower extremity joints and muscle groups in the human locomotor system alter mechanical functions to meet task demand. *Journal of Experimental Biology, 222*(20), jeb206383. doi:10.1242/jeb.206383

Leardini, A. & Caravaggi, P. (2017). Kinematic Foot Models for Instrumented Gait Analysis. *Handbook for Human Motion*, 1-24. doi:10.1007/978-3-319-30808-1_28-1

MacWillimas, B. A., Cowley, M., & Nicholson, D. E. (2003). Foot Kinematics And Kinetics During Adolescent Gait. *Gait & Posture*, 214-224. doi:https://doi.org/10.1016/S0966-6362(02)00103-0

Morasso, P. G. & Schieppati, M. (1999). Can Muscle Stiffness Alone Stabilize Upright Standing? *Journal of Neurophysiology, 82*(3), 1622-1626. doi:https://doi.org/10.1152/jn.1999.82.3.1622

Neptune, R. R., Sasaki, K., & Kautz, S. A. (2008). The Effect Of Walking Speed On Muscle Function And Mechanical Energetics. *Gait & Posture*, 135-143. doi:https://doi.org/10.1016/j.gaitpost.2007.11.004

Olney, S. J. (1991). Work and power in gait of stroke patients. *Archives of Physical Medicine and Rehabilitation, 72*(5), 309-314. doi:https://doi.org/10.5555/uri:pii:000399939190247G

Schwartz, M. H., Rozumalski, A., & Trost, J. P. (2008). The effect of walking speed on the gait of typically developing children. *Journal of Biomechanics*, 1639-1650. doi:https://doi-org.ezproxy.uvu.edu/10.1016/j.jbiomech.2008.03.015

Scott, S. H. & Winter, D. A. (1993). Biomechanical Model of the Human Foot: Kinematics and Kinetics During the Stance Phase of Walking. *Journal of Biomechanics, 26*(9), 1091-1104. doi:https://doi.org/10.1016/S0021-9290(05)80008-9

Stefanyshyn, D. J. & Nigg, B. M. (1997). Mechanical Energy Contribution of the Metatarsophalangeal Joint to Running and Sprinting. *Journal of Biomecahnics*, 1081-1085. doi:https://doi.org/10.1016/S0021-9290(97)00081-X

Stucke, S., McFarland, D., Goss, L. F., McMillan, G. R., Tucker, A., & Davis, B. L. (2012). Spatial relationships between shearing stresses and pressure on the plantar skin surface during gait. *Journal of Biomechanics, 45*(2), 619-622. doi:https://doi.org/10.1016/j.jbiomech.2011.11.004

Suzuki, J., Tanaka, Y., Takaoka, T., Kadono, K., & Takakura, Y. (2004). Axial radiographic evaluation in hallux valgus: evaluation of the transverse arch in the forefoot. *Journal of Orthopaedic Science*. doi:https://doi.org/10.1007/s00776-004-0800-9

Zajac, F. E., Neptune, R. R., & Kautz, S. A. (2002a). Biomechanics And Muscle Coordination Of Human Walking Part I: Introduction To Concepts, Power Transfer, Dynamics And Simulations. *Gait & Posture,* (16), 215-232. doi:https://doi.org/10.1016/S0966-6362(02)00068-1

Zajac, F. E., Neptune, R. R., & Kautz, S. A. (2002b). Biomechanics And Muscle Coordination Of Human Walking Part Ii: Lessons From Dynamical Simulations And Clinical Implications. *Gait & Posture*, 1-17. doi:https://doi.org/10.1016/S0966-6362(02)00069-3

Zelik, K. E., Takahashi, K. Z., & Sawicki, G. S. (2015). Six degree-of-freedom analysis of hip, knee, ankle and foot provides updated understanding of biomechanical work during human walking. *Journal of Experimental Biology, 6*(218), 876-886. doi:10.1242/jeb.115451

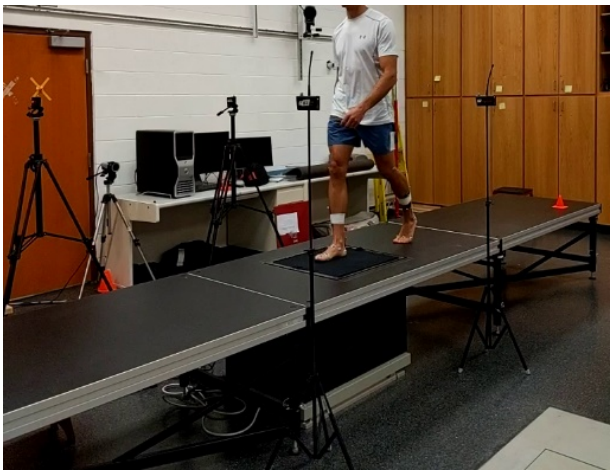

Figure 1. Participant on walkway. A 5.5 m long walkway was modified by cutting a hole in the center so that the pressure/shear sensor was flush with the walking surface. The timing lights for speed measurements are also visible.

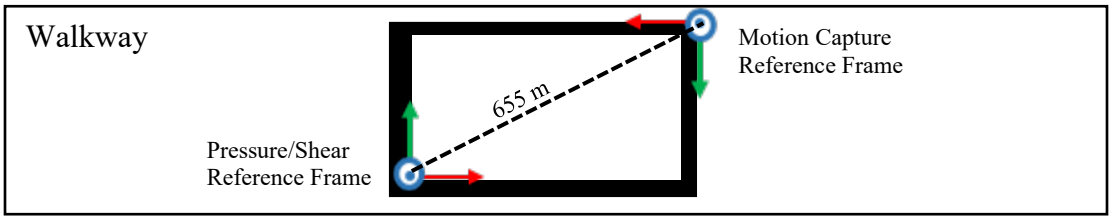

Figure 2. Spatial alignment. The walkway (outer white rectangle) with the FootSTEPS device (black rectangle) and pressure/shear measurement film (inner white rectangle). The pressure/shear reference frame is located at the lower left corner of the film while the motion capture reference frame is located at the upper right corner of the device. The offset measured between reference frame origins is provided (1.02 m longitudinally and 1.16 m laterally).

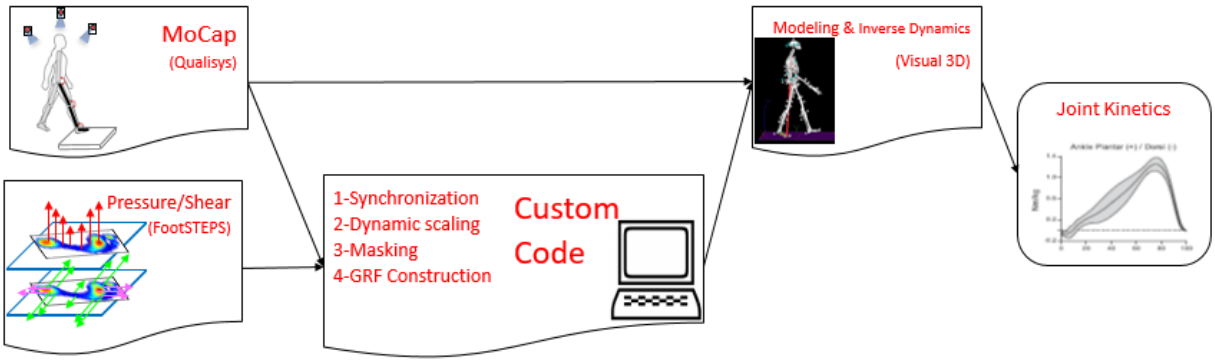

Figure 3. Visual workflow of system integration. Motion capture and pressure/shear data were collected simultaneously and imported into custom software. Four main integration steps were accomplished and final segment GRFs were exported. GRFs and motion capture were then imported into Visual 3D software for modeling and inverse dynamics, resulting in foot joint kinetics.

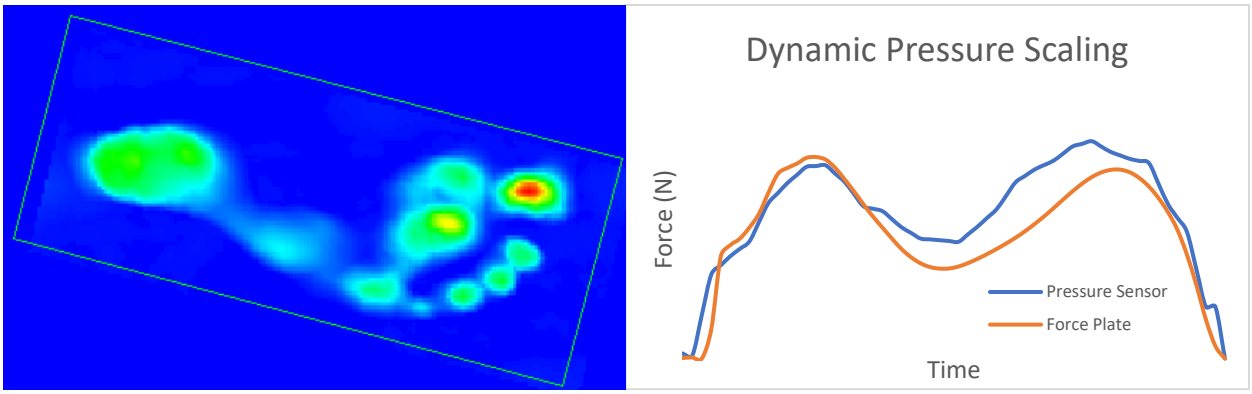

A B

Figure 4. Dynamic pressure scaling. Representative composite pressure image and an extracted foot region (A). The region of interest was defined from motion capture markers superimposed onto the composite image. The total vertical force from this region is shown along with the vertical force plate signal from the same trial (B), prior to dynamic scaling.

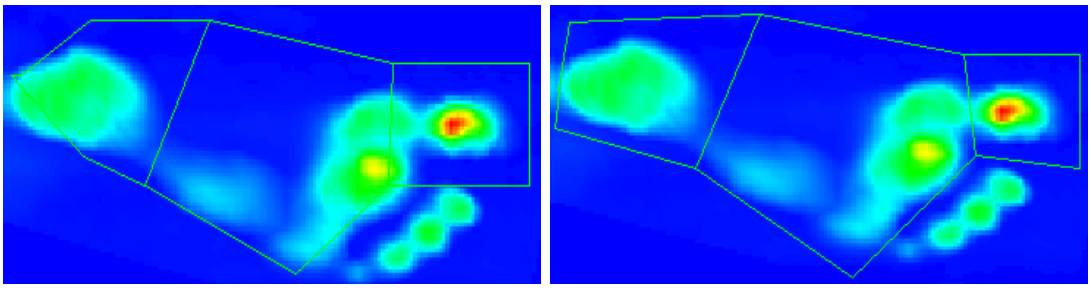

A B

Figure 5. Segmental masking. A representative example of anatomical masking which created straight lines between motion capture marker positions that incorrectly represent model segments (A). Manual masking corrected this error to include the valid pressure data (B).

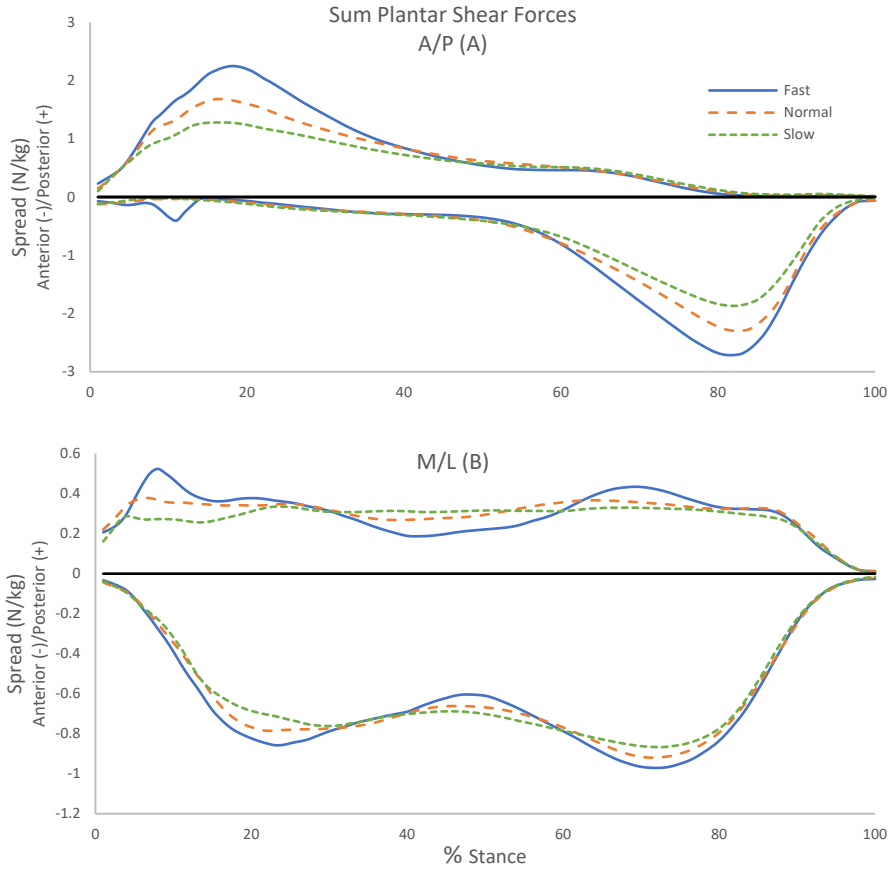

Figure 6. Opposing plantar shear stresses. Sum shear forces in each direction are shown. Vertical axis represents shear force normalized to bodyweight. Horizontal axis represents percent stance phase. Colors represent means at slow, normal, and fast walking speeds, 1.0, 1.3, and 1.6 m/s respectively.

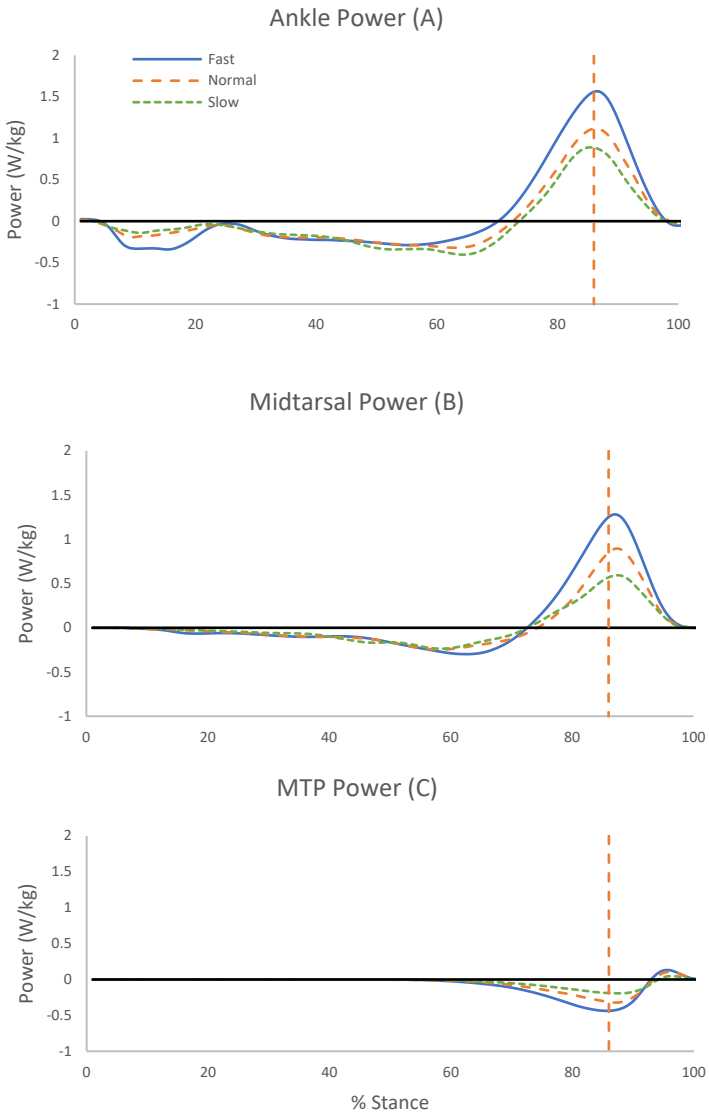

Figure 7. Joint powers. Vertical axis represents joint power normalized to bodyweight (W/kg). Horizontal axis represents percent stance phase. Colors represent the mean power at slow, normal, and fast walking speeds, 1.0, 1.3, and 1.6 m/s respectively. Vertical line represents peak ankle power at the normal walking speed.

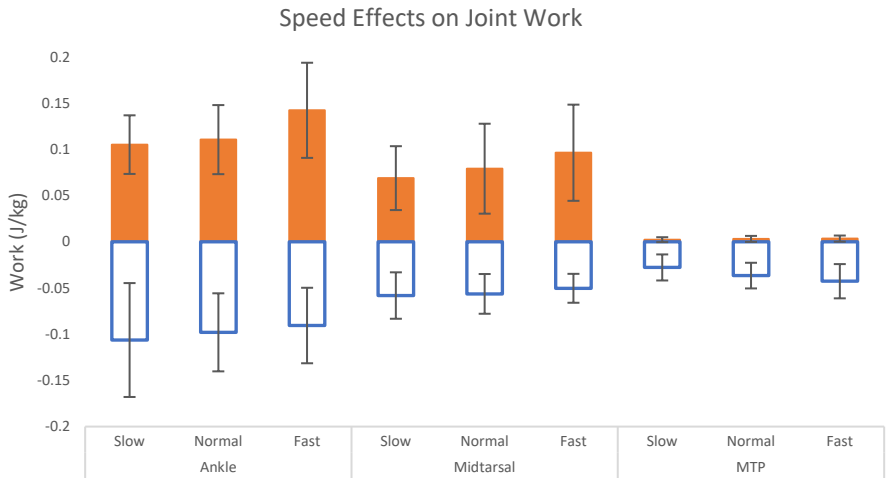

Figure 8. Joint work. Vertical axis represents joint work done during stance normalized to bodyweight (J/kg). Horizontal axis represents individual joints separated by walking speed. Solid orange boxes indicate the mean positive work and hollow blue boxes represent the mean negative work. Standard deviations are shown as error bars.

Appendix

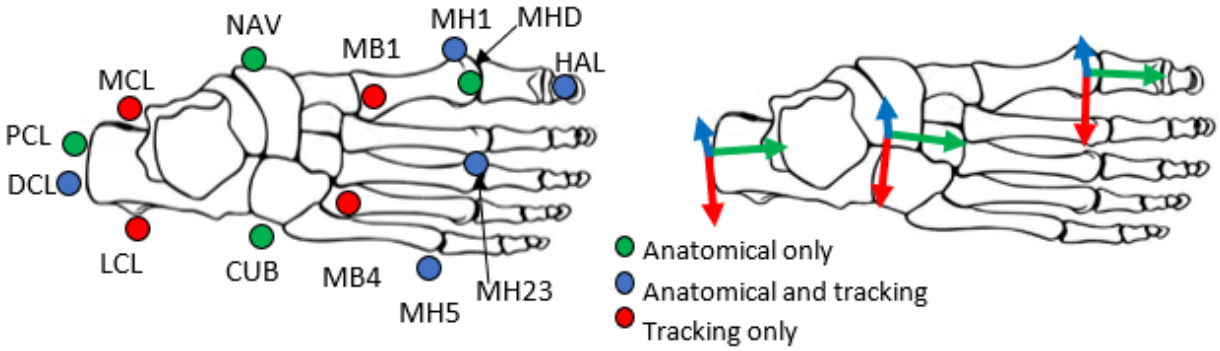

Kinetic Multisegment Foot Model Description

Figure A1: Marker placement diagram (left). Segment reference frame diagram (right).

Table A1: Marker placement descriptions and virtual marker definitions.

Symbol	Description
Markers	
DCL	Distal Calcaneus - apex of calcaneal tuberosity
PCL	Proximal Calcaneus – placed vertically in line between RDCL and RPCL, bisect calcaneus
LCL	Lateral calcaneus
MCL	Medial calcaneus
NAV	Superior prominence of navicular bone
CUB	Centroid of cuboid bone
MB1	Dorsal surface near 1st metatarsal base
MB4	Dorsal surface near 4th metatarsal base
MH1	Medial aspect of 1st metatarsal head
MH5	Lateral aspect of 5th metatarsal head
MH23	Dorsal surface, midway between 2nd and third metatarsal heads
MHD	Dorsal aspect of 1st metatarsal head
HAL	Center of hallux nail
Virtual Landmarks	
MJC	Midtarsal joint center – midpoint between CUB, NAV
FF_Dist	Forefoot distal end – project MH23 down to average height of MH1 and MH5
MTPC	1st MTP joint center – project MHD ½ distance to floor
HAL_Dist	Hallux distal end – Project HAL ½ distance to floor
MTPC_Track	MTPC tracked by Forefoot Segment
MHD_Track	MHD tracked by Forefoot Segment
MHD_Proj	MHD_Track projected laterally in plane of HAL, MTPC_Track, MHD_Track

Table A2: Model segment reference frame definitions.

Segment	Long axis	Plane	Tracking Markers
Hindfoot	DCL to MJC	DCL, MJC, PCL (Sagittal)	DCL, MCL, LCL
Forefoot	MJC to FF_Dist	MJC, FF_Dist, MH23 (Sagittal)	MB1,MB4, MH23, MH5, MH1
Hallux	MPC to HX_Dist	MPC, HX_Dist, H1 (Sagittal)	HAL, MTPC_Track, MHD_Proj